OPEN ACCESS
IOP Publishing
Journal of Physics A: Mathematical and Theoretical
J. Phys. A: Math. Theor. **56** (2023) 505202 (27pp)
https://doi.org/10.1088/1751-8121/ad0a71

# NOON state measurement probabilities and outcome fidelities: a Bethe ansatz approach

**Lachlan Bennett*, Phillip S Isaac and Jon Links**

School of Mathematics and Physics, The University of Queensland, St Lucia, QLD 4072, Australia

E-mail: lachlan.bennett@uqconnect.edu.au

Received 30 June 2023; revised 31 October 2023
Accepted for publication 7 November 2023
Published 27 November 2023

**Abstract**

A recently proposed extended Bose–Hubbard model, one that is a quantum integrable model, provides a framework for a NOON state generation protocol. Here we derive a Bethe ansatz solution for the model. The form of the solution provides the means to obtain exact asymptotic expressions for the energies and eigenstates. These results are used to derive formulae for measurement probabilities and outcome fidelities. We benchmark these results against numerical calculations.

Keywords: NOON state, quantum integrability, Bethe ansatz, fidelity

(Some figures may appear in colour only in the online journal)

## 1. Introduction

The NOON state [1] is a fundamental quantum state, one that has been promoted for applications in quantum metrology and sensing [2–4]. It also has the potential to play a wider role in quantum information processing [5, 6]. While a majority of initial studies focused on photonic NOON states [7, 8], it is in principle possible to also achieve a NOON state through the use of massive particles [9]. For example, the massive analog of the simplest type of NOON

* Author to whom any correspondence should be addressed.

state has been experimentally verified in a Bose–Einstein condensate setting, through the Hong–Ou–Mandel effect [10].

A NOON state is an entangled state that takes the form

$$|\psi_{\mathrm{NOON}}\rangle = \frac{1}{\sqrt{2}}|N,0\rangle + \frac{\mathrm{e}^{\mathrm{i}\phi}}{\sqrt{2}}|0,N\rangle,$$

representing a superposition where all particles simultaneously occupy one of two quantum states. In Dowling's comprehensive survey [11] on the role and significance of NOON states in optical metrology, he gives credit to Barry Sanders for first discussing NOON states [12]. That 1989 paper was interested in the Schrödinger cat aspect and how that affected quantum decoherence; although the term 'NOON state' itself was not coined until 2002 in [1] as a footnote. NOON states were rediscovered as a solution to surpass the classical diffraction limit in optical lithography [13]. Their properties have been used in quantum interferometry, with initial proposals and experimental methods focusing on entangled photons in delayed-choice experiments [14]. The following years witnessed advancements in techniques to produce NOON states. One approach involves super-resolution phase measurements using multi-photon entangled states [15]. Another approach is the mixing of quantum and classical light, which presents a new path to create high-NOON states (NOON states where $N$ is large) [7].

There has been a variety of recent proposals to manufacture NOON states that include the use of trapped ions [16], waveguide arrays [17], ultracold bosons [18–20], double-slit interference [21], magnons [22], cavity quantum electrodynamics (QED) [23], and circuit QED [24]. One proposal for massive NOON state generation uses a system of dipolar atoms confined to a four-site lattice [25, 26]. This setup affords the tunability of the system's coupling parameters through the dipole interactions. For particular choices of parameters the system becomes quantum integrable, which in turn opens up the means to investigate the model at a deep mathematical level. A key finding in [25, 26] is that, in the so-called *resonant tunnelling* regime, an initial Fock state of the integrable system will evolve to a state that is close to the so-called *über*-NOON state. This state is one that will collapse to a NOON state under a particular projective measurement.

It is important to observe that the procedure described above is fundamentally different from spin-squeezing proposals to generate NOON-type correlations through evolution under the one-axis twisting Hamiltonian of Kitagawa and Udea [27]. For example, the recent studies [28, 29] appeal to internal degrees of freedom in the constituents of an interacting system to generate NOON-type correlations via Greenberger–Horne–Zeilinger states. By contrast, the protocol of our study is one whereby the NOON correlations are with respect to spatial bosonic degrees of freedom.

Associated with the quantum integrability of the model is access to an exact solution through Bethe ansatz methods. One such solution was derived in [30], using the procedure known as the quantum inverse scattering method. Here we take a different approach to derive an alternative form of the Bethe ansatz solution. Our motivation for undertaking this route is that this new form readily permits the identification of leading-order terms of *all* eigenstates and eigenenergies. This in turn facilitates the calculation of the dynamical evolution of the system in the resonant tunnelling regime. In particular, we use these results to derive formulae for measurement probabilities and outcome fidelities. We then compare these results against complementary numerical studies and discuss their relationships.

In section 2 we introduce the extended Bose–Hubbard model (EBHM) on four lattice sites, and describe the Fock space of states on which it acts. We also provide a brief and intuitive description of its integrability. In section 3 we review how the model is used to implement the

NOON-state protocol. A Bethe ansatz method is proposed in section 4 to obtain expressions for the eigenvalues and eigenstates of the Hamiltonian. Using series expansions we obtain the leading-order terms of these quantities. This then enables expressions to be computed for the dynamic time evolution of the system from an initial Fock input state. Section 5 provides a detailed analysis to derive formulae for the measurement probabilities and outcome fidelities associated with the protocol of section 3. We examine a variety of scenarios for the choice of coupling parameters in order to identify the limits of applicability of these results. In particular, we expose different time-scales for oscillations in the dynamics and argue that high-frequency oscillating terms have small amplitude and can generally be ignored. Concluding remarks are given in section 6.

## 2. Quantum integrable four-site Bose–Hubbard model

A four-site EBHM will be used to describe the physics of interacting dipolar bosons on a plaquette. In addition to the boson interaction within sites, the model accounts for the interaction of bosons between sites; required to accommodate the dipole interactions [31]. This is a modification to the familiar Bose–Hubbard model [32]. The EBHM Hamiltonian reads

$$H=\frac{U_0}{2}\sum_{i=1}^{4}N_i\left(N_i-1\right)+\sum_{i=1}^{4}\sum_{j=1,j\neq i}^{4}\frac{U_{ij}}{2}N_iN_j-\frac{J}{2}\left[a_1^\dagger a_2+a_1^\dagger a_4+a_3^\dagger a_2+a_3^\dagger a_4+\text{h.c.}\right], \tag{1}$$

where h.c. denotes the hermitian conjugate, $U_0$ is the coupling for short-range interactions of particles within the same site, and $U_{ij}=U_{ji}$ are the long-range couplings for interactions between sites [31, 33]. The Hamiltonian also has tunnelling terms, which are set to be equal to $J$ for nearest-neighbour sites.

Basis vectors for the Hilbert space of states are taken to be Fock states defined as follows:

$$|n_1,n_2,n_3,n_4\}=\frac{\left(a_1^\dagger\right)^{n_1}}{\sqrt{n_1!}}\frac{\left(a_2^\dagger\right)^{n_2}}{\sqrt{n_2!}}\frac{\left(a_3^\dagger\right)^{n_3}}{\sqrt{n_3!}}\frac{\left(a_4^\dagger\right)^{n_4}}{\sqrt{n_4!}}|0\rangle,$$

where the vacuum state $|0\rangle$ is the normalised vector satisfying $a_i|0\rangle=0$. The creation and annihilation operators for bosons, denoted by $a_i^\dagger$ and $a_i$ respectively, act on the $i$th site. These operators obey the commutation relations:

$$\left[a_i,a_j^\dagger\right]=\delta_{ij},\quad [a_i,a_j]=\left[a_i^\dagger,a_j^\dagger\right]=0,\quad i,j=1,2,3,4.$$

Additionally, the operator $N_i=a_i^\dagger a_i$, called the number operator, determines the occupation number at site $i$. The sum of these operators, $N=\sum_{i=1}^{4}N_i$, is called the total number operator. For this quantum system, the total number operator is conserved as the total number of bosons remains constant.

Furthermore, this Hamiltonian is *quantum integrable* when $U_{13}=U_{24}=U_0$ and $U_{12}=U_{14}=U_{23}=U_{34}$. Up to conserved constant terms, this gives us the following integrable model

$$H=U\left(N_1+N_3-N_2-N_4\right)^2-\frac{J}{2}\left[\left(a_1^\dagger+a_3^\dagger\right)\left(a_2+a_4\right)+\left(a_2^\dagger+a_4^\dagger\right)\left(a_1+a_3\right)\right], \tag{2}$$

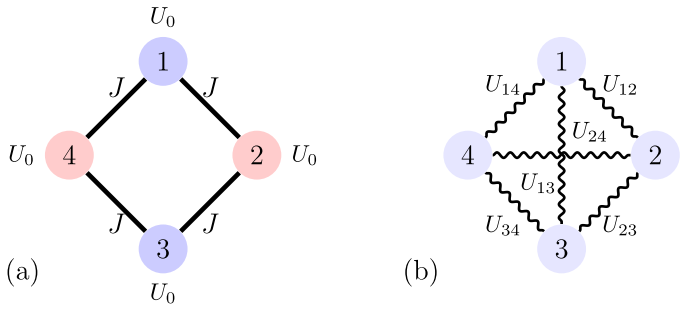


**Figure 1.** Schematic representation of the four-site extended Bose–Hubbard model (1). (a) The Bose–Hubbard model depicting four lattice sites with alternating red and blue colours, representing the bipartite structure of the graph. The tunnelling strength between neighbouring sites is denoted by $J$, and the on-site bosonic interaction strength is $U_0$. (b) Inclusion of inter-site bosonic interactions $U_{ij}$ results in the extended Bose–Hubbard model.

where $U = (U_{12} - U_0)/4$ [26]. Exchanging indices $\{1,3\}$ with $\{2,4\}$ preserves the Hamiltonian (2), accentuating an inherent bipartite symmetry. Also, the tunnelling between lattice sites can be represented by the bipartite graph $K_{2,2}$ [34], see figure 1. As formulated, (2) acts on the Hilbert space $V_N$:

$$V_N = \left\{ |n_1, n_2, n_3, n_4\} \middle| \quad n_1 + n_2 + n_3 + n_4 = N \right\},$$

for some fixed number of bosons $N$. Notably, the dimensions of these Hilbert spaces are the tetrahedral numbers,

$$\dim(V_N) = \frac{(N+1)(N+2)(N+3)}{6}.$$

### *2.1. Canonical transformation*

Although the model (2) can be derived through the quantum inverse scattering method [30], ensuring solvability via the algebraic Bethe ansatz, we can demonstrate its quantum integrability explicitly by first implementing a canonical transformation,

$$b_1^\dagger = \frac{1}{\sqrt{2}}\left(a_1^\dagger + a_3^\dagger\right), \quad b_3^\dagger = \frac{1}{\sqrt{2}}\left(a_1^\dagger - a_3^\dagger\right)$$
$$b_2^\dagger = \frac{1}{\sqrt{2}}\left(a_2^\dagger + a_4^\dagger\right), \quad b_4^\dagger = \frac{1}{\sqrt{2}}\left(a_2^\dagger - a_4^\dagger\right).$$

Since the transformation is unitary, and is therefore an isomorphism on a finite-dimensional vector space, the Fock states

$$|n_1, n_2, n_3, n_4\rangle = \frac{\left(b_1^\dagger\right)^{n_1}}{\sqrt{n_1!}} \frac{\left(b_2^\dagger\right)^{n_2}}{\sqrt{n_2!}} \frac{\left(b_3^\dagger\right)^{n_3}}{\sqrt{n_3!}} \frac{\left(b_4^\dagger\right)^{n_4}}{\sqrt{n_4!}} |0\rangle,$$

are also basis vectors for the Hilbert space $V_N$. Consequently, the Hamiltonian can be re-expressed using these new operators:

$$H = U\left(\tilde{N}_1 + \tilde{N}_3 - \tilde{N}_2 - \tilde{N}_4\right)^2 - J\left(b_1^\dagger b_2 + b_2^\dagger b_1\right), \tag{3}$$

where $\tilde{N}_i = b_i^\dagger b_i$. There are four mutually commuting conserved operators,

$$\left[\tilde{N}_3, \tilde{N}_4\right] = \left[\tilde{N}_i, H\right] = \left[\tilde{N}_i, N\right] = 0, \quad i = 3,4.$$

This model is integrable, as there are four degrees of freedom and we have identified four conserved quantities: the Hamiltonian $H$ and the operators $\tilde{N}_3$, $\tilde{N}_4$, and $N$. This basis allows us to represent the conserved operators $\tilde{N}_3$ and $\tilde{N}_4$ as number operators.

Quantum integrability also simplifies the analysis by transforming from a four-site Bose–Hubbard Hamiltonian to an ensemble of two-mode Hamiltonians:

$$H_{l,m} = U\left(\tilde{N}_1 + l - \tilde{N}_2 - m\right)^2 - J\left(b_1^\dagger b_2 + b_2^\dagger b_1\right), \tag{4}$$

for all pairs of integers $l, m \in \mathcal{I} = \{l, m \in \mathbb{Z}_+ : N - l - m \geqslant 0\}$. We can represent the four-site Hamiltonian as the direct sum

$$H = \bigoplus_{l,m \in \mathcal{I}} H_{l,m}.$$

This matches the observation found from the algebraic Bethe ansatz; finding a one-to-one correspondence between the Bethe ansatz equations for the integrable EBHM (2) and the Bethe ansatz equations for the two-mode Bose–Hubbard models (4) [30]. Understanding the Hamiltonian in this way provides us with a framework needed to apply an alternative Bethe ansatz technique.

Foremost, the objective of this paper is to provide corrections to the leading-order terms in the NOON state fidelities and outcome probabilities pertaining to the NOON state protocol developed in [25, 26]. The following section provides: an articulation of the general problem of producing a NOON state in mathematical terms; an outline of the specific NOON state protocol we will analyse; and a brief summary of how NOON states apply to interferometry.

## 3. NOON state protocol

Mathematically, the task of creating a NOON state can be summarised as follows: given some initial vector, $|\psi\rangle$, one must find a unitary operator $U(t)$ such that for

$$U(t)\,|\psi\rangle = \sum_{k=0}^{N} c_k(t)\,|\psi_k(t)\rangle,$$

there exists a time $\tau$ where $c_0(\tau)|\psi_0(\tau)\rangle = (1/\sqrt{2})|N,0\rangle$, $c_N(\tau)|\psi_N(\tau)\rangle = (1/\sqrt{2})\mathrm{e}^{\mathrm{i}\phi}|0,N\rangle$ and $c_1(\tau) = \ldots = c_{N-1}(\tau) = 0$. One difficulty is finding a unitary operator that describes a physical process for massive particles; the majority of experimental techniques and proposals for generating NOON states have made use of the manipulation of photons.

### *3.1. Protocol*

In [25, 26] a proposal was put forth for the creation of NOON states, not by the manipulation of photons, but by the control of ultra-cold atoms; inspired by recent advancements in the field of atomtronics [35]. Fortunately, the nature of entanglement allows a NOON state to be created without being restricted to a two-site model. We can identify a state in which the collapse of one subsystem, by a projective measurement, results in an entangled state within the complementary subsystem. This has been found to be the case for the four-site EBHM. For the initial state $|L,M,0,0\}$, where the total number of bosons $N=L+M$ is odd[1], a measurement can be made on site 3 at the time

$$\tau = 2\pi\, U\,(L-M+1)\,(L-M-1)\,/J^2 \tag{5}$$

to produce a NOON state across sites 2 and 4. However, this is not an exact NOON state as this result was derived using an effective Hamiltonian, not the Hamiltonian (2). In [25], it was observed that large energy degeneracies exist for the Hamiltonian (2) when $J=0$, and that for small values of $J/U$ the energy levels stratify into well-defined bands. Informed by this structure, the effective Hamiltonian was derived through second-order tunnelling processes:

$$H_{\text{eff}} = (N+1)\,\Omega\left(\tilde{N}_3+\tilde{N}_4\right) - 2\Omega\tilde{N}_3\tilde{N}_4 \tag{6}$$

where $\Omega=\pi/(2\tau)$, and is valid for the resonant tunnelling regime characterised by $J \ll U|L-M|$. The spectrum of $H_{\text{eff}}$ follows as

$$E_{\text{eff}} = (N+1)\,\Omega\,(l+m) - 2\Omega lm,$$

for $l=0,\ldots,L$ and $m=0,\ldots,M$. Moreover, it was shown that when considering the time-evolved state, $\exp(-iH_{\text{eff}}t)|L,M,0,0\}$, the time $t=\tau$ corresponds to

$$\begin{aligned}\exp\left(-iH_{\text{eff}}\tau\right)|L,M,0,0\} = \frac{(-1)^{\frac{(N+1)}{2}}}{2}|L,M,0,0\} + \frac{1}{2}|L,0,0,M\} + \frac{1}{2}|0,M,L,0\} \\ + \frac{(-1)^{\frac{(N-1)}{2}}}{2}|0,0,L,M\}.\end{aligned} \tag{7}$$

We will refer to this specific entangled state (7) as the *über-NOON* state. Given an über-NOON state, taking a measurement on either site 1 or site 3 will produce one of two possible NOON states across sites 2 and 4:

$$|\Psi_{\text{NOON}};(0)_3\} = \frac{(-1)^{\frac{(N+1)}{2}}}{\sqrt{2}}|L,M,0,0\} + \frac{1}{\sqrt{2}}|L,0,0,M\}, \tag{8}$$

$$|\Psi_{\text{NOON}};(L)_3\} = \frac{1}{\sqrt{2}}|0,M,L,0\} + \frac{(-1)^{\frac{(N-1)}{2}}}{\sqrt{2}}|0,0,L,M\}, \tag{9}$$

where the notation $(0)_3$ or $(L)_3$ is used to denote 0 or $L$ number of bosons at site 3. After measurement, both NOON states may occur with a probability of $1/2$. To clearly demonstrate that these are NOON states, consider (8) written in the form

[1] The protocol does not work when $N$ is even. Dependence on the parity of the total number of particles, in the study of time evolution of systems involving NOON states, has also been observed in [36].

$$|\Psi_{\mathrm{NOON}};(0)_3\} = \left(\frac{(-1)^{\frac{(N+1)}{2}}}{\sqrt{2}}|M\}_2|0\}_4 + \frac{1}{\sqrt{2}}|0\}_2|M\}_4\right)\otimes|L\}_1|0\}_3;$$

this is what is meant by producing a NOON state over sites 2 and 4. Likewise, measuring either site 2 or site 4 produces one of two possible NOON states:

$$|\Psi_{\mathrm{NOON}};(0)_4\} = \frac{(-1)^{\frac{(N+1)}{2}}}{\sqrt{2}}|L,M,0,0\} + \frac{1}{\sqrt{2}}|0,M,L,0\},$$
$$|\Psi_{\mathrm{NOON}};(M)_4\} = \frac{1}{\sqrt{2}}|L,0,0,M\} + \frac{(-1)^{\frac{(N-1)}{2}}}{\sqrt{2}}|0,0,L,M\},$$

this time over sites 1 and 3. Throughout, we adopt the convention to make a measurement on site 3, as taking a measurement on site 1 will produce the same set of NOON states, and measuring either sites 2 or 4 is equivalent to taking a measurement on site 3 with the transformation $L \leftrightarrow M$.

This protocol outlines the time evolution of a specific class of initial states into über-NOON states. By taking a measurement on site 3 a NOON state is produced, which can be symmetric or anti-symmetric, each with an outcome probability of $1/2$. However, the proposed experimental apparatus for this protocol better reflects the physics described by the EBHM Hamiltonian (1) rather than the effective Hamiltonian (6). Fortunately, by applying a Bethe ansatz technique (refer to section 4), we can study the time evolution of states under the four-site EBHM Hamiltonian. In section 5 we analyse this protocol, quantifying how closely it produces NOON states via a fidelity calculation, and estimating the outcome probabilities based on this alternative time evolution definition.

### 3.2. *Interferometry*

This subsection should be treated as a brief digression to discuss how the system is capable of interferometry; for more details, we refer the reader to [26]. In [26], the proposition was made that the quantum integrable four-site EBHM could be physically realised using ultracold dipolar atoms, trapped in an optical lattice. This allows for the encoding of a phase to be implemented by the application of an external field, temporarily breaking integrability, but undertaken in a small enough time interval to have minimal loss of fidelity. Suppose that by using the NOON state protocol we produce a symmetric $|\Psi_{\mathrm{NOON}};(0)_4\}$ state ($(N+1)/2$ is even). Once a phase $\phi = M\theta$ is encoded we can examine the evolution of the initial state

$$|\Phi(\phi)\} = \frac{1}{\sqrt{2}}|L,M,0,0\} + \frac{\exp(i\phi)}{\sqrt{2}}|L,0,0,M\}. \tag{10}$$

If the expectation value of an observable, $\mathcal{O}$, is dependent on $\theta$, then the value of $\theta$ can be estimated. Moreover, using standard estimation theory [1, 3, 6], the uncertainty in estimating the parameter can be measured; i.e. the precision $\Delta\theta$, where $\Delta$ is the standard deviation. In this case, the observable used for estimating $\theta$ is the *imbalance* between sites 1 and 3. Given an initial state (10), the evolved state $|\Phi(\phi)(\tau)\} = \exp(-iH_{\mathrm{eff}}\tau)|\Phi(\phi)\}$ has the imbalance expectation value (see [26])

$$\langle(N_1 - N_3)(\tau)\rangle = \{\Phi(\phi)(\tau)|(N_1 - N_3)|\Phi(\phi)(\tau)\} = (-1)^{\frac{(N+1)}{2}} L\cos(M\theta).$$

Using the error propagation formula [1, 3], it is seen that the system achieves Heisenberg-limited phase sensitivity since

$$\Delta\theta = \frac{\Delta\langle (N_1 - N_3)(\tau)\rangle}{|\partial_\theta \langle (N_1 - N_3)(\tau)\rangle|} = \frac{1}{M}.$$

It is impossible for a non-entangled state to reach this level of precision (as the above outperforms the shot-noise limit $\Delta\theta \sim 1/\sqrt{M}$), demonstrating a clear advantage quantum technology has over classical systems for metrology [2, 37].

## 4. The Bethe ansatz

For implementing the Bethe ansatz, we will denote the eigenvalues of $\tilde{N}_3$ and $\tilde{N}_4$ as $l$ and $m$, respectively. Consider

$$V_{N,l,m} = \mathrm{Span}\left(\{|N-l-m,0,l,m\rangle, |N-l-m-1,1,l,m\rangle, \ldots, |0,N-l-m,l,m\rangle\}\right),$$

the space $V_N$ can be expressed as a direct sum of all possible spaces $V_{N,l,m}$ ($l$ and $m$ must be positive integers and $N-l-m \geqslant 0$). Since we have that for all $|\psi\rangle \in V_{N,l,m}$, $H|\psi\rangle \in V_{N,l,m}$, we must have the eigenstates as elements in the vector space $V_{N,l,m}$. In section 2, it was already explained how the eigenspectrum has a one-to-one correspondence to a particular ensemble of two-mode Bose–Hubbard Hamiltonians. This allows us to implement methods previously used in analysing the two-site model. It is known that the eigenvectors for the two-site model can be expressed in the form $|\Psi\rangle = \prod_{n=1}^{N}(u_n b_1^\dagger + b_2^\dagger)|0\rangle$, where each $u_n \in \mathbb{C}$ is some parameter. A natural modification for the four-site model would be to assume the form

$$|\Psi\rangle = \prod_{n=1}^{N-l-m}\left(u_n b_1^\dagger + b_2^\dagger\right)|0,0,l,m\rangle. \tag{11}$$

This assumption can be justified by the fact that any vector $|\psi\rangle \in V_N$ can be expressed in terms of a linear combination $|\psi\rangle = \sum_{n=0}^{N-l-m}\alpha_n (b_1^\dagger)^{N-l-m-n}(b_2^\dagger)^n|0,0,l,m\rangle$, which is an alternative form to (11).

### 4.1. The Bethe ansatz equations

The eigenvalue equation, $H|\Psi\rangle = E|\Psi\rangle$, can be used to find the constraints we need to impose on the free parameters, $\{u_n : n = 1,\ldots,N-l-m\}$, of $|\Psi\rangle$. We rewrite the Hamiltonian (3) as

$$H = U\left(\tilde{N}_1 - \tilde{N}_2\right)^2 + U\left(\tilde{N}_3 - \tilde{N}_4\right)^2 + 2U\left(\tilde{N}_3 - \tilde{N}_4\right)\left(\tilde{N}_1 - \tilde{N}_2\right) - J\left(b_2^\dagger b_1 + b_1^\dagger b_2\right).$$

By construction we have $\tilde{N}_3|\Psi\rangle = l|\Psi\rangle$ and $\tilde{N}_4|\Psi\rangle = m|\Psi\rangle$. The actions of other operators on $|\Psi\rangle$ are calculated to be

$$
\begin{aligned}
b_1^\dagger b_2|\Psi\rangle &= \sum_{n=1}^{N-l-m} b_1^\dagger|\Psi_n\rangle,\\
b_2^\dagger b_1|\Psi\rangle &= \sum_{n=1}^{N-l-m} u_n|\Psi\rangle - \sum_{n=1}^{N-l-m} u_n^2 b_1^\dagger|\Psi_n\rangle,\\
\left(\tilde{N}_1-\tilde{N}_2\right)|\Psi\rangle &= 2\sum_{n=1}^{N-l-m} u_n b_1^\dagger|\Psi_n\rangle - (N-l-m)|\Psi\rangle,\\
\left(\tilde{N}_1-\tilde{N}_2\right)^2|\Psi\rangle &= 4(N-l-m-1)\sum_{n=1}^{N-l-m} u_n b_1^\dagger|\Psi_n\rangle - 8\sum_{n=1}^{N-l-m}\sum_{r=1,r\neq n}^{N-l-m}\frac{u_n^2}{u_n-u_r}b_1^\dagger|\Psi_n\rangle\\
&\quad + (N-l-m)^2|\Psi\rangle,
\end{aligned}
$$

where $|\Psi_n\rangle = \prod_{j=1,j\neq n}^{N-l-m}(u_j b_1^\dagger + b_2^\dagger)|0,0,l,m\rangle$. We now substitute this into the eigenvalue equation and match up the states $|\Psi\rangle$ to find that

$$
E = U(N-2l)^2 - J\sum_{n=1}^{N-l-m} u_n. \tag{12}
$$

We are then left with the $|\Psi_n\rangle$ states. To satisfy $H|\Psi\rangle = E|\Psi\rangle$ we set each coefficient of $|\Psi_n\rangle$ to zero. This condition gives us

$$
\frac{J}{4U}u_n^{-2} + (1-N+2m)u_n^{-1} - \frac{J}{4U} = \sum_{r=1,r\neq n}^{N-l-m}\frac{2}{u_r-u_n}, \quad \forall n = 1,\ldots,N-l-m, \tag{13}
$$

the Bethe ansatz equations, where $\{u_n : n = 1,\ldots,N-l-m\}$ is the set of solutions; which we will refer to as Bethe roots.

**Remark.** Alternatively, one can come to the same set of equations by making the association,

$$
S^+ = b_1^\dagger b_2, \quad S^- = b_1^\dagger b_1, \quad S^z = \frac{1}{2}\left(\tilde{N}_1+\tilde{N}_2\right),
$$

which gives the $su(2)$ relations,

$$
\left[S^z, S^\pm\right] = \pm S^\pm, \quad \left[S^+, S^-\right] = 2S^z.
$$

Using a differential operator realisation we can express the Hamiltonian as a second-order differential acting on a $(N-l-m+1)$-dimensional space of polynomials. In this formulation, the Bethe ansatz equation (13) are derived from the Hamiltonian acting on an arbitrary polynomial $Q(x)$ of order $N-l-m$, written in terms of its roots $\{u_n\}$ as $Q(x) = \prod_{n=1}^{N-l-m}(x-u_n)$ [38].

### *4.2. Asymptotic solution*

The expression for the spectrum (12) of the Hamiltonian only relies on the sum of Bethe roots $\sum_{n=1}^{N-l-m} u_n$. We can obtain an expression for this sum up to order $J/U$, which gives a formula for the eigenspectrum up to order $J^2/U$. In deriving this expression from the Bethe ansatz equations, we will assume the condition $J/U \ll 1$, such that higher-order terms can be treated as negligible. Before making any further assumptions, observe that by multiplying the Bethe ansatz equations (13) by $u_n$ and then summing over all of the roots,

$$\frac{J}{4U}\sum_{n=1}^{N-l-m} u_n^{-1} + (1-N+2m)(N-l-m) - \frac{J}{4U}\sum_{n=1}^{N-l-m} u_n = \sum_{n=1}^{N-l-m}\sum_{r=1,r\neq n}^{N-l-m}\frac{2u_n}{u_r-u_n} = -(N-l-m)(N-l-m-1),$$

we derive an identity relating the sum of all roots to the sum of the inverse roots,

$$J\sum_{n=1}^{N-l-m} u_n = J\sum_{n=1}^{N-l-m} u_n^{-1} + 4U(N-l-m)(m-l). \tag{14}$$

**Remark.** The identity (14) implies that for when $l=m$ we have $\sum_{n=1}^{N-2m} u_n = \sum_{n=1}^{N-2m} u_n^{-1}$. This is in accordance with the fact that when $l=m$ the Bethe ansatz equations have a $u_n \leftrightarrow u_n^{-1}$ symmetry. Furthermore, this symmetry implies the stronger condition that, in this case, both solution sets $\{u_n : n=1,\ldots,N-2m\}$ and $\{u_n^{-1} : n=1,\ldots,N-2m\}$ are identical.

Equation (14) allows an alternative expression for the eigenvalues (12),

$$\begin{aligned} E &= U(N-2l)^2 - J\sum_{n=1}^{N-l-m} u_n \\ &= U(N-2l)^2 - J\sum_{n=1}^{N-l-m} u_n^{-1} - 4U(N-l-m)(m-l) \\ &= U(N-2m)^2 - J\sum_{n=1}^{N-l-m} u_n^{-1}. \end{aligned}$$

Note that for this to hold, we can conclude that, in general, the series $\sum_{n=1}^{N-l-m} u_n$ and $\sum_{n=1}^{N-l-m} u_n^{-1}$ diverge as $J$ approaches zero, such that $J\sum_{n=1}^{N-l-m} u_n$ and $J\sum_{n=1}^{N-l-m} u_n^{-1}$ remain finite. Therefore, we will assume that we can split the Bethe roots into two categories,

$$u_n = \begin{cases} O(U/J), & 1 \leqslant n \leqslant p, \\ O(J/U), & p < n \leqslant N-l-m, \end{cases} \tag{15}$$

where the roots are distinguished by their leading-order behaviour. The first $p$ Bethe roots, $\{u_n : n=1,\ldots,p\}$, are referred to as *large* because they are roots of leading-order $U/J$ and those

remaining, $\{u_n : n = p+1,\ldots,N-l-m\}$, are *small* roots as they are order $J/U$. Expressing the summation as

$$\sum_{n=1}^{N-l-m} u_n = \sum_{n=1}^{p} u_n + \sum_{n=p+1}^{N-l-m} u_n,$$

the goal is to separately calculate expressions for both $\sum_{n=1}^{p} u_n$ and $\sum_{n=p+1}^{N-l-m} u_n$. Starting with the sum over large roots, we take an arbitrary Bethe ansatz equation where $u_n$ is large,

$$\frac{J}{4U}u_n^{-2} + (1-N+2m)\,u_n^{-1} - \frac{J}{4U} = \sum_{r=1,r\neq n}^{N-l-m} \frac{2}{u_r - u_n}$$

$$\frac{J}{4U}u_n^{-2} + (1-N+2m)\,u_n^{-1} - \frac{J}{4U} = \underbrace{\sum_{r=1,r\neq n}^{p} \frac{2}{u_r - u_n}}_{\text{large roots}} + \underbrace{\sum_{r=p+1}^{N-l-m} \frac{2}{u_r - u_n}}_{\text{small roots}}.$$

Next, we take a series expansion of the second summation (corresponding to small roots) and then neglect all higher-order terms, leading to

$$\frac{J}{4U}u_n^{-2} + (1-N+2m)\,u_n^{-1} - \frac{J}{4U} = \sum_{r=1,r\neq n}^{p} \frac{2}{u_r - u_n} - 2u_n^{-1}(N-l-m-p) + O\left(J^2/U^2\right)$$

$$(1-N+2m)\,u_n^{-1} - \frac{J}{4U} \approx \sum_{r=1,r\neq n}^{p} \frac{2}{u_r - u_n} - 2u_n^{-1}(N-l-m-p).$$

We have used the '$\approx$' notation to indicate an equivalence up to and including terms of leading order $J/U$. We then sum over all large roots to obtain the final expression,

$$(1-N+2m)\sum_{n=1}^{p} u_n^{-1} - \frac{J}{4U}p \approx \sum_{n=1}^{p}\sum_{r=1,r\neq n}^{p} \frac{2}{u_r - u_n} - 2(N-l-m-p)\sum_{n=1}^{p} u_n^{-1}$$

$$(N-2l-2p+1)\sum_{n=1}^{p} u_n^{-1} - \frac{J}{4U}p \approx 0,$$

$$\sum_{n=1}^{p} u_n^{-1} \approx \frac{J}{4U}\frac{p}{N+1-2l-2p}. \tag{16}$$

Likewise, a similar procedure can be applied to find the sum over all small roots,

$$\sum_{n=p+1}^{N-l-m} u_n \approx -\frac{J}{4U}\frac{N-l-m-p}{N-1-2l-2p}. \tag{17}$$

However, (16) is an expression for the sum of inverse roots, not $\sum_{n=1}^{p} u_n$. Fortunately, much like in the derivation of the identity (14), we can sum over the equation

$$\frac{J}{4U}u_n^{-1} + (1-N+2m) - \frac{J}{4U}u_n = \sum_{r=1,r\neq n}^{p} \frac{2u_n}{u_r-u_n} + \sum_{r=p+1}^{N-l-m} \frac{2u_n}{u_r-u_n},$$

to find the relation between the sum of large roots and the sum of their inverses,

$$\sum_{n=1}^{p} u_n \approx \sum_{n=1}^{p} u_n^{-1} + \frac{4U}{J}(N-2l-p)p + \frac{8U}{J}\left(\sum_{n=1}^{p} u_n^{-1}\right)\left(\sum_{r=p+1}^{N-l-m} u_r\right).$$

### *4.3. Eigenvalues and eigenstates*

Now that we have an expression for the sum over Bethe roots, $\sum_{n=1}^{N-l-m} u_n$, we can substitute this into (12) to acquire a formula for the eigenvalues of this model as a function of $l, m$ and $p$,

$$E_{p,l,m} \approx U(N-2l-2p)^2 + \frac{J^2}{4U}\left[\frac{(N-l-m-p)(N+1-2l) - p(N-1-2l-2p)}{(N-2l-2p)^2-1}\right].$$

In this context, the '$\approx$' represents an equivalency up to order $J^2$. To match each eigenvalue with its corresponding eigenstate we apply the expressions we have calculated to the unnormalised eigenstates,

$$|\Psi_{p,l,m}\rangle = \frac{1}{\sqrt{p!\,(N-l-m-p)!}} \prod_{n=1}^{p}\left(b_1^\dagger + u_n^{-1}b_2^\dagger\right) \prod_{n=p+1}^{N-l-m}\left(u_n b_1^\dagger + b_2^\dagger\right)|0,0,l,m\rangle,$$

as we can approximate this vector up to order $J/U$,

$$\begin{aligned}|\Psi_{p,l,m}\rangle \approx |p,N-l-m-p,l,m\rangle &+ \sqrt{\frac{N+1-l-m-p}{p}}\sum_{n=1}^{p} u_n^{-1}|p-1,N-l-m-p+1,l,m\rangle \\ &+ \sqrt{\frac{p+1}{N-l-m-p}}\sum_{n=p+1}^{N-l-m-p} u_n|p+1,N-l-m-p-1,l,m\rangle.\end{aligned}$$

Conveniently, all $J/U$ terms in our approximation are exactly determined by (16) and (17), giving the formula

$$\begin{aligned}|\Psi_{p,l,m}\rangle \approx |p,N-l-m-p,l,m\rangle &+ \frac{J}{4U}\frac{\sqrt{p(N+1-l-m-p)}}{N+1-2l-2p}|p-1,N-l-m-p+1,l,m\rangle \\ &- \frac{J}{4U}\frac{\sqrt{(p+1)(N-l-m-p)}}{N-2l-2p-1}|p+1,N-l-m-p-1,l,m\rangle.\end{aligned}$$

The following section studies the quantum dynamics of the system. Specifically, we are interested in analysing the NOON state protocol; pertaining to the time evolution of the state $|L,M,0,0\}$. To achieve this, it is convenient to make a change of variables, matching the formalism outlined in the protocol. Let $L=l+p$ and $M=N-L$, where $l=0,\ldots,L$ and $m=0,\ldots,M$, this gives us expressions for the eigenvalues and eigenstates in terms of $L,M,l$ and $m$,

$$E_{L,M,l,m} \approx U(L-M)^2 + \frac{J^2}{4U}\left[\frac{-(L+M+1)(l+m)+2lm+L(L+1)+M(M+1)}{(L-M)^2-1}\right], \tag{18}$$

$$|\Psi_{L,M,l,m}\rangle \approx |L-l,M-m,l,m\rangle - \frac{J}{4U}\frac{\sqrt{(L-l)(M-m+1)}}{L-M-1}|L-l-1,M-m+1,l,m\rangle$$
$$- \frac{J}{4U}\frac{\sqrt{(L-l+1)(M-m)}}{M-L-1}|L-l+1,M-m-1,l,m\rangle. \tag{19}$$

This change of variables clearly displays the $L\leftrightarrow M$ and $l\leftrightarrow m$ symmetries of the eigenvalue formula and is indicative of the $(L,l)\leftrightarrow(M,m)$ symmetry of the whole quantum system. It is clear that equations (18) and (19) are singular if $|L-M|=1$. In this instance the assumption (15) is not valid, we find that there are roots of order $(J/U)^0$. Hereafter it will be assumed $|L-M|\neq 1$.

## 5. Measurement probabilities and outcome fidelities

### 5.1. Quantum dynamics

We can now determine the time evolution dynamics for a given initial quantum state in the four-site EBHM. For an arbitrary number of particles $N$, we have derived exact formulae for the leading order terms of both the eigenvalues and eigenstates. This allows us to accurately determine the quantum dynamics of the system. The time evolution of a quantum system is described by Schrödinger's equation,

$$i\frac{\partial|\psi\rangle}{\partial t} = H|\psi\rangle.$$

Since the Hamiltonian (2) is independent of time we have the solution to the equation,

$$|\psi(t)\rangle = \mathrm{e}^{-\mathrm{i}Ht}|\psi(0)\rangle = \sum_{n=1}^{N}\mathrm{e}^{-\mathrm{i}E_n t}|\Psi_n\rangle\langle\Psi_n|\psi(0)\rangle,$$

where $|\Psi_n\rangle$ is the eigenstate corresponding to the eigenvalue $E_n$. Having derived complete sets of eigenvalues $\{E_{L,M,l,m}\}$ and eigenvectors $\{|\Psi_{L,M,l,m}\rangle\}$, this allows us to accurately determine the state $\exp(-iH\tau)|L,M,0,0\} = |L,M,0,0;(\tau)\}$,

$$|L,M,0,0;(\tau)\} = \sum_{L',M'=0}^{N}\sum_{l=0}^{L'}\sum_{m=0}^{M'}\delta^N_{L'+M'}\frac{\exp(-i\tau E_{L',M',l,m})}{\mathcal{N}^2_{L',M',l,m}}|\Psi_{L',M',l,m}\rangle\langle\Psi_{L',M',l,m}|L,M,0,0\},$$

up to order $J/U$, providing order $J^2/U^2$ corrections to the über-NOON state (7). In the above expression, $\mathcal{N}^2_{L',M',l,m}$ normalises the projections $|\Psi_{L',M',l,m}\rangle\langle\Psi_{L',M',l,m}|$,

$$\begin{aligned}\mathcal{N}^2_{L,M,l,m} &= \langle\Psi_{L,M,l,m}|\Psi_{L,M,l,m}\rangle \\ &\approx 1+\frac{J^2}{16U^2}\left(\frac{(L-l)(M-m+1)}{(L-M-1)^2}+\frac{(M-m)(L-l+1)}{(L-M+1)^2}\right).\end{aligned}$$

Using the derived expression for the eigenstates (18) and the normalisation factors, we can determine that the time-evolved initial state (up to terms of order $J^2/U^2$) is given by

$$\begin{aligned}|L,M,0,0;(\tau)\} \approx &\sum_{l=0}^{L}\sum_{m=0}^{M}\alpha_{l,m}(\tau)\,|L-l,M-m,l,m\rangle \\ &-\frac{J}{4U(L-M+1)}\sum_{l=0}^{L+1}\sum_{m=0}^{M-1}\beta_{l,m}(\tau)\,|L-l+1,M-m-1,l,m\rangle \\ &-\frac{J}{4U(M-L+1)}\sum_{l=0}^{L-1}\sum_{m=0}^{M+1}\gamma_{l,m}(\tau)\,|L-l-1,M-m+1,l,m\rangle \quad (20)\end{aligned}$$

where

$$\begin{aligned}\alpha_{l,m}(\tau) = &\Big[\exp\left(-i\tau E_{L,M,l,m}\right) \\ &+\frac{J^2}{16U^2(L-M+1)^2}(L-l+1)(M-m)\left(\exp\left(-i\tau E_{L+1,M-1,l,m}\right)-\exp\left(-i\tau E_{L,M,l,m}\right)\right) \\ &+\frac{J^2}{16U^2(M-L+1)^2}(L-l)(M-m+1)\left(\exp\left(-i\tau E_{L-1,M+1,l,m}\right)-\exp\left(-i\tau E_{L,M,l,m}\right)\right)\Big] \\ &\times\sqrt{\frac{L!M!}{2^{L+M}(L-l)!l!(M-m)!m!}},\end{aligned}$$

$$\beta_{l,m}(\tau) = (L-l+1)\left(\exp\left(-i\tau E_{L+1,M-1,l,m}\right)-\exp\left(-i\tau E_{L,M,l,m}\right)\right)\sqrt{\frac{L!M!}{2^{L+M}(L-l+1)!l!(M-m-1)!m!}},$$

$$\gamma_{l,m}(\tau) = (M-m+1)(\exp(-i\tau E_{L-1,M+1,l,m})-\exp(-i\tau E_{L,M,l,m}))\sqrt{\frac{L!M!}{2^{L+M}(L-l-1)!l!(M-m+1)!m!}}.$$

It is worth noting that the über-NOON state coincides with the leading-order expression which excludes all terms order $J/U$ and higher. That is

$$\begin{aligned}&|L,M,0,0;(\tau)\} \\ &\underset{\text{leading-order}}{\approx}\sum_{l=0}^{L}\sum_{m=0}^{M}\exp\left(-i\tau E_{L,M,l,m}\right)\sqrt{\frac{L!M!}{2^{L+M}(L-l)!l!(M-m)!m!}}\,|L-l,M-m,l,m\rangle \\ &\quad = |\ddot{u}ber\text{-NOON}\},\end{aligned}$$

where $|\ddot{u}ber\text{-NOON}\}$ is given by equation (7).

### 5.2. Über-NOON state fidelity

We will quantify the proximity of the evolved state $|L,M,0,0;(\tau)\}$ to the desired über-NOON state. We can do this by calculating the über-NOON state fidelity, defined as $\mathcal{F} = |\{\ddot{u}ber\text{-NOON}|L,M,0,0;(\tau)\}|$ . This fidelity is an expression in terms of $\alpha_{l,m}(\tau)$,

$$\begin{aligned}\mathcal{F} \approx \Bigg| & \frac{(-1)^{\frac{(N+1)}{2}}}{2}\sum_{l=0}^{L}\sum_{m=0}^{M}\alpha_{l,m}(\tau)\sqrt{\frac{L!M!}{2^{L+M}l!(L-l)!m!(M-m)!}} \\ & + \frac{1}{2}\sum_{l=0}^{L}\sum_{m=0}^{M}\alpha_{l,m}(\tau)(-1)^{m}\sqrt{\frac{L!M!}{2^{L+M}l!(L-l)!m!(M-m)!}} \\ & + \frac{1}{2}\sum_{l=0}^{L}\sum_{m=0}^{M}\alpha_{l,m}(\tau)(-1)^{l}\sqrt{\frac{L!M!}{2^{L+M}l!(L-l)!m!(M-m)!}} \\ & + \frac{(-1)^{\frac{(N-1)}{2}}}{2}\sum_{l=0}^{L}\sum_{m=0}^{M}\alpha_{l,m}(\tau)(-1)^{l+m}\sqrt{\frac{L!M!}{2^{L+M}l!(L-l)!m!(M-m)!}}\Bigg|. \end{aligned} \tag{21}$$

Using the following identities:

$$\begin{aligned}\exp(-i\tau E_{L,M,l,m}) &= (-1)^{\frac{(N+1)}{2}}\exp\left(-i\tau U(L-M)^2\right)\exp\left(i\pi\left(lm-\frac{(N+1)}{2}(l+m)\right)\right), \\ \exp(-i\tau E_{L+1,M-1,l,m}) &= (-1)^{\frac{(N+1)}{2}}\exp\left(-i\tau(L-M)^2\right)\exp(-i\tau 4U(L-M+1)) \\ &\quad\times\exp\left(i\pi\left(lm-\frac{(N+1)}{2}(l+m)\right)\right)z^{(N+1)(l+m)-2lm-\sigma}, \\ \exp(-i\tau E_{L-1,M+1,l,m}) &= (-1)^{\frac{(N+1)}{2}}\exp(-i\tau(L-M)^2)\exp(i\tau 4U(L-M-1)) \\ &\quad\times\exp(i\pi(lm-\frac{(N+1)}{2}(l+m)))\bar{z}^{(N+1)(l+m)-2lm-\overline{\sigma}},\end{aligned}$$

where $z=\exp(-i2\pi/(L-M+3))$, $\bar{z}=\exp(i2\pi/(L-M-3))$, $\sigma=(L+1)(L+2)+M(M-1)$ and $\overline{\sigma}=L(L-1)+(M+1)(M+2)$, this expression can be simplified to

$$\begin{aligned}\mathcal{F} \approx \Bigg| & 1-\frac{J^2}{16U^2(L-M+1)^2}\frac{M(L+2)}{4}-\frac{J^2}{16U^2(L-M-1)^2}\frac{L(M+2)}{4} \\ & + \exp(-i\tau 4U(L-M+1))\frac{J^2}{16U^2(L-M+1)^2}\frac{M}{2^{L+M}}z^{-\sigma}\sum_{l=0}^{L}z^{(N+1)l}\left(1+z^{(N+1)-2l}\right)^{M-1}\frac{(L-l+1)L!}{l!(L-l)!} \\ & + \exp(i\tau 4U(L-M-1))\frac{J^2}{16U^2(L-M-1)^2}\frac{L}{2^{L+M}}\bar{z}^{-\overline{\sigma}}\sum_{m=0}^{M}\bar{z}^{(N+1)m}\left(1+\bar{z}^{(N+1)-2m}\right)^{L-1}\frac{(M-m+1)M!}{m!(M-m)!}\Bigg|. \end{aligned} \tag{22}$$

One observation is that the über-NOON fidelity formula has a reducible part, which simplifies to a closed-form expression, and an irreducible part, remaining expressed as a summation. Furthermore, we can recognise that the irreducible part describes how the über-NOON fidelity oscillates as a function of $J/U$, and that the reducible part describes an average around which

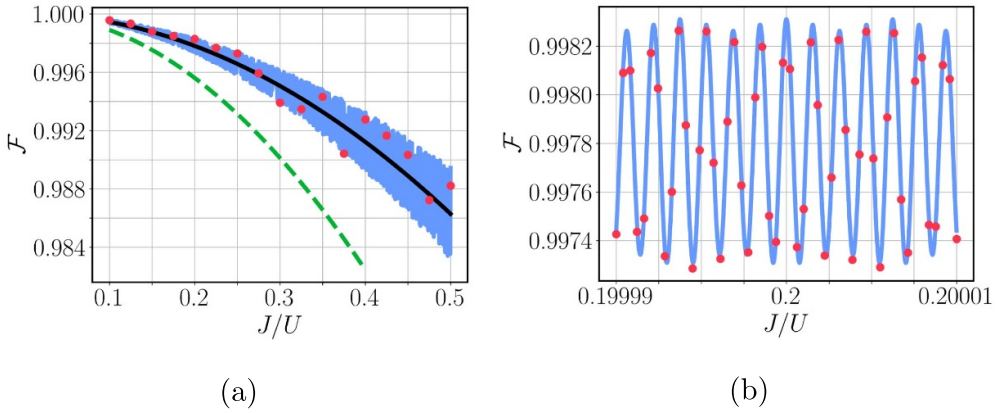


**Figure 2.** Comparison of analytic expressions and numerical data for the über-NOON fidelity. The above graphs compare derived expressions for the über-NOON fidelity, as a function of $J/U$, to the über-NOON fidelity derived from the numerical diagonalisation of the Hamiltonian. For this example, we have chosen the values $L=7$ and $M=16$. (a) The first graph plots numerical data (red dots) for $J/U$ ranging from 0.1 to 0.5. We compare the data to the derived über-NOON state fidelity formula (22) (solid oscillating blue line) and the reducible part of the über-NOON fidelity expression (23) (solid black line). Also displayed is the über-NOON fidelity lower bound (24) (dashed green line). (b) In the second graph, we zoom in around $J/U=0.2$, plotting the analytic formula (22) alongside 50 numerical data points.

the function oscillates. One might recognise that the $1/2^{L+M}$ factors of the irreducible expressions imply that these terms diminish for large values of $L$ and $M$; the oscillations dampen. This implies that the reducible, or *non-oscillating* part of the expression

$$\mathcal{F}_{\text{non-oscillating}} \approx 1 - \frac{J^2}{16U^2\left(L-M+1\right)^2}\frac{M\left(L+2\right)}{4} - \frac{J^2}{16U^2\left(M-L+1\right)^2}\frac{L\left(M+2\right)}{4}, \tag{23}$$

serves as an increasingly useful estimation. As displayed in figure 2(a), we also observe that (23) improves as an estimate when the value of $J/U$ decreases. With the values of $L$ and $M$ held constant ($L=7$, $M=16$), we discern that a higher $J/U$ value results in an increased variance of oscillation. Another observation suggests that we can derive a straightforward expression for a lower-bound

$$1 - \frac{J^2}{16U^2\left(L-M+1\right)^2}\frac{M\left(L+2\right)}{2} - \frac{J^2}{16U^2\left(L-M-1\right)^2}\frac{L\left(M+2\right)}{2} \leqslant \mathcal{F}, \tag{24}$$

using the triangle inequality and acknowledging that $|z| = |\bar{z}| = 1$. However, the conditions for the lower bound must adhere to the conditions that make the derivations valid: namely, $L+M$ is odd and $|L-M| \neq 1$. We also still require that $J/U < 1$ be sufficiently small. It is more accurate to say that we have established a lower bound on all the über-NOON fidelity terms up to and including leading order $J^2/U^2$. Conceivably, for $J/U$ large enough, this inequality could be broken if we are to include higher-order terms. Note, however, that the subsequent higher-order term is of order $J^4/U^4$, not $J^3/U^3$, signifying the robustness of the order $J^2/U^2$ approximation. Considering that the tunnelling regime aligns with high-frequency formulae, a lower bound proves useful in scenarios involving high oscillation variance, which happens for some smaller values of $L$ and $M$.

### *5.3. Measurement probabilities and NOON state fidelities*

Thus far, we have computed an expression approximating the über-NOON fidelity; a measure estimating the proximity of the time-evolved state, $|L,M,0,0;(\tau)\}$ (20), to über-NOON state (7). This serves as an effective proxy measure for the overall NOON state protocol, as the über-NOON state guarantees the generation of a NOON state following a projective measurement. Nevertheless, NOON state fidelities offer a more direct evaluation of the protocol. To formulate these fidelities, we first define a state $|L,M,0,0;(\tau)(r)_3\}$ as the state $|L,M,0,0;(\tau)\}$ after measuring site 3 and observing $r$ bosons. Therefore, we can simply define the NOON fidelities by,

$$\mathcal{F}_3(0) = |\left\{\Psi_{\text{NOON}};(0)_3|L,M,0,0;(\tau)(0)_3\right\}|, \mathcal{F}_3(L) = |\left\{\Psi_{\text{NOON}};(L)_3|L,M,0,0;(\tau)(L)_3\right\}|,$$

where the NOON states are defined by (8) and (9) respectively. When a measurement outcome that is neither 0 or $L$ is obtained we conclude that the output state does not resemble a NOON state; these attempts can be immediately dismissed. Therefore, assuming we can accurately approximate success probabilities, NOON state fidelities provide a more precise evaluation of the NOON state protocol compared to the über-NOON fidelity. Although these fidelities are computed in a manner similar to the über-NOON fidelity derivation, we require the measurement probabilities $\mathbb{P}_3[0](\tau)$ and $\mathbb{P}_3[L](\tau)$:

$$\begin{aligned}\mathbb{P}_3[0](\tau) = &\sum_{l,l'=0}^{L}\sum_{m=0}^{M}\alpha_{l,m}(\tau)\alpha^*_{l',m}(\tau)\frac{L!}{2^L\sqrt{(L-l)!l!(L-l')!l'!}}\\ &+\frac{J^2}{16U^2(L-M+1)^2}\sum_{l,l'=0}^{L+1}\sum_{m=0}^{M-1}\beta_{l,m}(\tau)\beta^*_{l',m}(\tau)\frac{(L+1)!}{2^{L+1}\sqrt{(L-l+1)!l!(L-l'+1)!l'!}}\\ &+\frac{J^2}{16U^2(M-L+1)^2}\sum_{l,l'=0}^{L-1}\sum_{m=0}^{M+1}\gamma_{1,m}(\tau)\gamma^*_{l',m}(\tau)\frac{(L-1)!}{2^{L-1}\sqrt{(L-l-1)!l!(L-l'-1)!l'!}}\end{aligned} \tag{25}$$

$$\begin{aligned}\mathbb{P}_3[L](\tau) = &\sum_{l,l'=0}^{L}\sum_{m=0}^{M}\alpha_{l,m}(\tau)\alpha^*_{l',m}(\tau)(-1)^{l+l'}\frac{L!}{2^L\sqrt{(L-l)!l!(L-l')!l'!}}\\ &+\frac{J^2}{16U^2(L-M+1)^2}\sum_{l,l'=0}^{L+1}\sum_{m=0}^{M-1}\beta_{l,m}(\tau)\beta^*_{l',m}(\tau)(-1)^{l+l'}\frac{(L-2l+1)(L-2l'+1)(L+1)!}{2^{L+1}\sqrt{(L-l+1)!l!(L-l'+1)!l'!}}.\end{aligned} \tag{26}$$

From the expression for $|L,M,0,0;(\tau)\}$ (20) and by normalising the wave function using the measurement probabilities, we can derive the NOON state fidelities to be

**Table 1.** Results obtained for an initial state $|4,11,0,0\}$ with measurement at site 3 taken at time $\tau$. This table compares numerical results (num) with the derived analytic expressions (an) for varying parameter values $J$ and $U$. The numerical data and chosen parameter values are selected from the supplementary material for the papers [25, 26]. Reproduced from [25]. CC BY 4.0.

| U/$\hbar$ (Hz) | J/$\hbar$ (Hz) | $\tau$ (s) | Meas. | Prob. (an) | Prob. (num) | Fid. (an) | Fid. (num) |
|---|---|---|---|---|---|---|---|
| 105.60 | 104.95 | 2.89 | 0 | 0.5028 | 0.4911 | 0.9329 | 0.9568 |
| 105.60 | 104.95 | 2.89 | 4 | 0.4688 | 0.4667 | 0.9929 | 0.9925 |
| 122.52 | 101.79 | 3.57 | 0 | 0.5066 | 0.4961 | 0.9751 | 0.9783 |
| 122.52 | 101.79 | 3.57 | 4 | 0.4766 | 0.4764 | 0.9951 | 0.9930 |
| 104.85 | 71.62 | 6.16 | 0 | 0.5044 | 0.4982 | 0.9841 | 0.9850 |
| 104.85 | 71.62 | 6.16 | 4 | 0.4850 | 0.4832 | 0.9967 | 0.9972 |

$$\mathcal{F}_3(0) = \left| \frac{1}{\sqrt{\mathbb{P}_3[0](\tau)}} \left[ \frac{(-1)^{\frac{(N+1)}{2}}}{\sqrt{2}} \sum_{l,m} \alpha_{l,m}(\tau) \sqrt{\frac{L!M!}{2^{L+M} l!(L-l)!m!(M-m)!}} \right.\right.$$
$$\left.\left. + \frac{1}{\sqrt{2}} \sum_{l,m} \alpha_{l,m}(\tau)(-1)^m \sqrt{\frac{L!M!}{2^{L+M} l!(L-l)!m!(M-m)!}} \right] \right|, \tag{27}$$

$$\mathcal{F}_3(L) = \left| \frac{1}{\sqrt{\mathbb{P}_3[L](\tau)}} \left[ \frac{1}{\sqrt{2}} \sum_{l,m} \alpha_{l,m}(\tau)(-1)^l \sqrt{\frac{L!M!}{2^{L+M} l!(L-l)!m!(M-m)!}} \right.\right.$$
$$\left.\left. + \frac{(-1)^{\frac{(N-1)}{2}}}{\sqrt{2}} \sum_{l,m} \alpha_{l,m}(\tau)(-1)^{l+m} \sqrt{\frac{L!M!}{2^{L+M} l!(L-l)!m!(M-m)!}} \right] \right| \tag{28}$$

Details on the derivation of the measurement probabilities (25) and (26) are found in the appendix.

To evaluate these formulae we have appealed to the supplementary material for both [25, 26]. Here we find numerical data for the probabilities and outcome fidelities where the chosen parameters for $U$ and $J$ were informed by the physical setup of the system, providing realistic values. In table 1, we have selected a few examples for an initial state $|4,11,0,0\}$ and compared the numerics to the derived analytic results. One key observation is that the analytic probability and fidelity estimate align more precisely with the numerical results when the measurement outcome is four bosons, in comparison to when the measurement outcome is 0. Moreover, the probability estimates for when the measurement outcome is 0 seem qualitatively different as all the estimates are greater than $1/2$; this feature of (25) alone is unexpected. However, our own numerical data confirms that it is possible to achieve a greater probability outcome than $1/2$, this is observed for the case where the values of $L$ and $M$ have been swapped—see figure 3 which plots $\mathbb{P}_3[0](\tau)$ for $L=11$ and $M=4$. An obvious issue could be that the parameter values for $U/J$ are too large, the lowest ratio being $J/U = 71.62/104.85 \approx 0.683\,07$. In figure 4, we plot the formulae and numerical data in a small neighbourhood around $J/U \approx 0.683\,07$. We compare this to the results in an even smaller neighbourhood, to account for a greater frequency, around a smaller value $J/U = 0.2$. Despite concern for the measurement 0 case, we observe that the formulae do match the numerical data (qualitatively in frequency and amplitude), only with a slight vertical shift. Unsurprisingly, changing $J/U$ to a smaller value yields much better results—note the $y$-axis scale of the graphs.

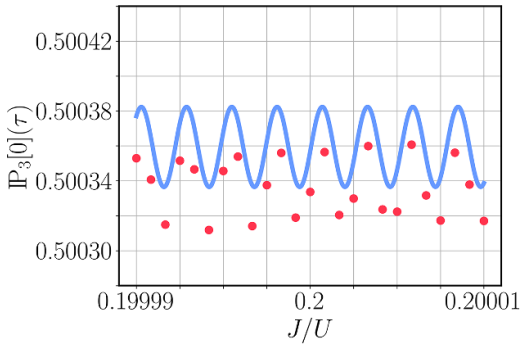


**Figure 3.** Probabilities greater than 0.5. $\mathbb{P}_3[0](\tau)$ (25) for $L = 11$, $M = 4$ around $J/U = 0.2$ (solid blue line) shows probabilities that are greater than 0.5. This unexpected property is confirmed by numerical data (red dots).

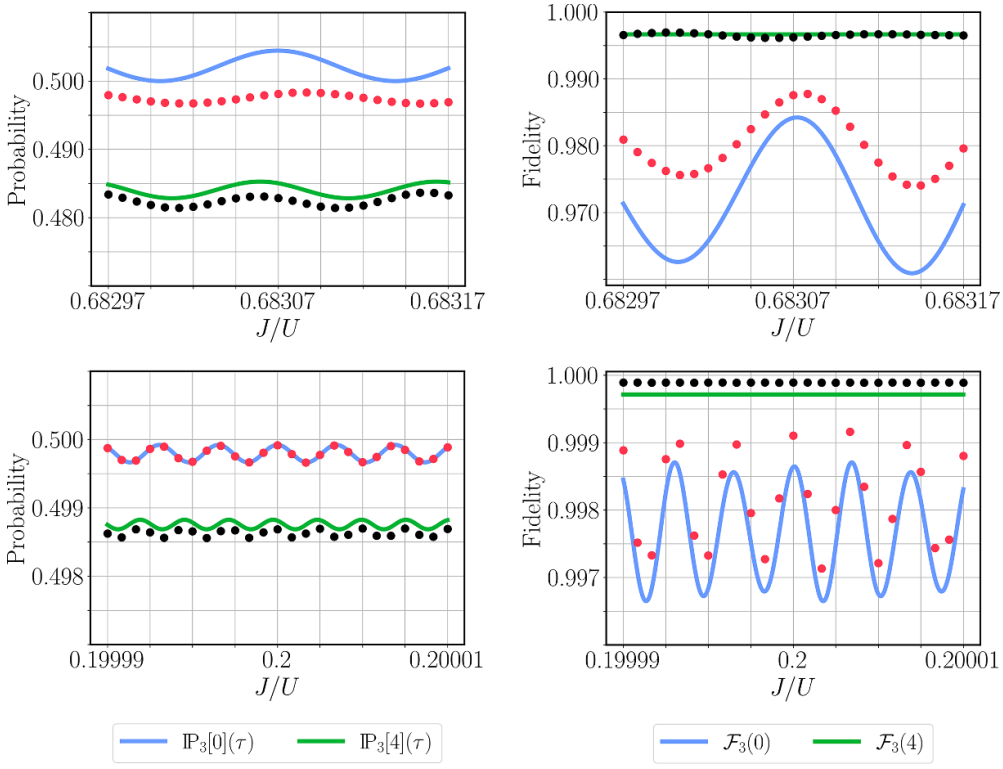


**Figure 4.** Probability and fidelity comparison for differing $J/U$ values. Consider the analytic formulae compared to the numerical results in table 1. The top graphs display the analytic expressions for the probabilities (25) and (26) and fidelities (27) and (28) compared with numerical data for $L = 4$, $M = 11$. These plots are centred around $J/U = 71.62/104.85 \approx 0.683\,07$. In the bottom graphs, the plots are centred around $J/U = 0.2$, all else is equal. Noting the scale of the vertical axes, the agreement between the analytic curves and the data points is excellent.

Similar to the über-NOON fidelity calculations, triple summations do not always simplify into a closed expression, but when they do not, they will reduce to one summation. For low limits of $L$ and $M$, each term in the derived expression is crucial. Computationally, this is not an issue when $L$ and $M$ are small, as there are fewer terms in the summations. However, as $L$ and $M$ increase, the number of terms to compute grows linearly, which may pose a problem. Intuitively, it might appear that the expressions become increasingly complex in the large $L, M$ limit, but this is not the case, as many terms become negligible, simplifying the formula in this limit.

### 5.4. Large $L, M$ limit

Finally, we come to a study of these results in the limit as $L$ and $M$ become large. In section 5.2 we discussed how the über-NOON state fidelity (22) has a reducible non-oscillating part and an irreducible oscillating part. The NOON state fidelities (27) and (28) and the measurement probabilities (25) and (26) also have this property. Moreover, we have already made the observation that as $L$ and $M$ become large, the oscillations in (22) dampen, leading to the approximation (23). Again, for all equations (25)–(28), as $L$ and $M$ increase, the oscillations dampen (see appendix). Only the reducible parts remain, specifically when the phase variables are integer multiples of $\pi/2$. In the *large $L, M$ limit*, oscillations become negligible, resulting in straightforward linear expressions (functions of $J^2/U^2$) to approximate the quantities (25)–(28). The formulae in the large $L, M$ limit are as follows:

$$\mathbb{P}_3[0](\tau) \approx \frac{1}{2} - \frac{J^2}{16U^2(L-M+1)^2}\frac{M(L+3)}{8} - \frac{J^2}{16U^2(M-L+1)^2}\frac{L(M+2)}{8} \tag{29}$$

$$\mathbb{P}_3[L](\tau) \approx \frac{1}{2} + \frac{J^2}{16U^2(L-M+1)^2}\frac{M}{8} - \frac{J^2}{16U^2(L-M+1)^2}\frac{M(L+2)}{4} - \frac{J^2}{16U^2(M-L+1)^2}\frac{L(M+2)}{4} \tag{30}$$

$$\mathcal{F} \approx 1 - \frac{J^2}{16U^2(L-M+1)^2}\frac{M(L+2)}{4} - \frac{J^2}{16U^2(M-L+1)^2}\frac{L(M+2)}{4} \tag{31}$$

$$\mathcal{F}_3(0) \approx 1 - \frac{J^2}{16U^2(L-M+1)^2}\frac{M(L+1)}{8} - \frac{J^2}{16U^2(M-L+1)^2}\frac{L(M+2)}{8} \tag{32}$$

$$\mathcal{F}_3(L) \approx 1 - \frac{J^2}{16U^2(L-M+1)^2}\frac{M}{8}. \tag{33}$$

Firstly, these formulae are functions of $J^2/U^2$, which is assumed to be small, based on the asymptotic solution to the sum of Bethe roots. From these formulae, we observe that the protocol's performance is maximised as $|L-M| \to \infty$. Regrettably, in this limit, if the increasing $|L-M|$ term is not counterbalanced by a diminishing tunnelling constant $J$, then $\tau \to \infty$; indicating that an improved performance takes a longer time. As a guideline, we can assume that $M$ is large and let $L = 2M$. This will satisfy the conditions that $L, M$ and $|L-M|$ are all large, ensuring the accuracy of the formulae. Moreover, these assumptions allow us to calculate the limits as $L \to \infty$. For example

$$\lim_{L\to\infty} \mathbb{P}_3[0](\tau) = \frac{1}{2} - \frac{J^2}{512U^2}.$$

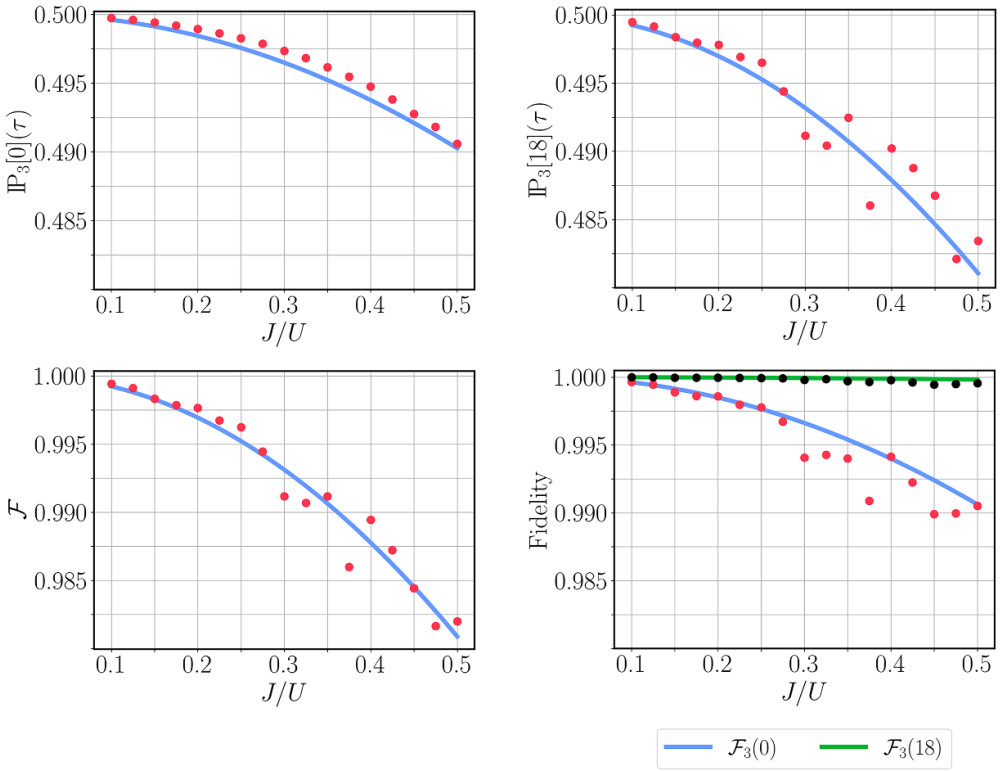


**Figure 5.** Large $L,M$ limit formulae. Plot of the large $L,M$ limit formulae equations (29)–(33) compared with numerical data. This is for values $L=18$ and $M=9$, and with $J/U$ ranging from 0.1 to 0.5.

In figure 5 we compare these formulae to numerical results where $J/U$ ranges from 0.1 to 0.5. Note that, for $L=18$ and $M=9$ leading to $N=27$, this is by no means a large $N$-value. Despite this, we can already observe that (30) and (31) appear to behave as the function the data oscillates around but the oscillations have not sufficiently dampened enough to provide a good estimate for higher values of $J/U$. For (29) the oscillations have dampened dramatically providing a reasonable estimate for this whole range of $J/U$ values. However, when evaluating (32) and (33) we note that our formulae seem to overestimate the average. This is due to the structure of the fidelity formulae where we take a square root (see (27) and (28)). Taking the square root of these oscillating terms leads to corrections that are of order $J^3/U^3$. We are observing here a greater sensitivity to higher-order terms. In this case either the values for $L$ and $M$ are too small or the values for $J/U$ are too large.

## 6. Summary and outlook

We have investigated the proposal for generating NOON states detailed in [25, 26], which employs a system of dipolar atoms confined to a four-site lattice. This system is described using the quantum integrable model characterised by the four-site EBHM given by equation (2).

Through the use of Bethe ansatz techniques, we derived exact formulae for the leading-order terms of all eigenvalues and eigenstates of this Hamiltonian via asymptotic techniques applied to the Bethe ansatz equations. After determining the eigenspectrum and the complete set of eigenstates, we analysed the time-evolution for the class of $|L,M,0,0\}$ initial states, where $N=L+M$ is odd, and derived higher-order expressions for outcome probabilities and fidelities associated with NOON-state generation. Additionally, we obtained simple formulae and fidelities in the large $L,M$ limit and validated our analytic results by comparing them with numerical calculations. These results obtained from the Bethe ansatz solution confirm that the NOON state protocol described is one that delivers high fidelity output states, exceeding 0.93 in all case studies, with a probability of success $\mathbb{P}_3(\tau)=\mathbb{P}_3[0](\tau)+\mathbb{P}_3[L](\tau)$ that is close to 1.

The results of this paper lay the groundwork for further research. For example, the Bethe ansatz techniques applied here can be extended to a broader class of generalised quantum integrable models [34]. This will expand knowledge of these systems, and extend capabilities in investigating bosonic networks. Furthermore, the techniques presented here provide a solid framework for exploring the dynamical properties of these general models. These results will be communicated in a future publication.

## Data availability statement

The data that support the findings of this study are available upon reasonable request from the authors.

## Acknowledgments

This work was supported by the Australian Research Council through Discovery Project DP200101339. The authors acknowledge the traditional owners of the land on which The University of Queensland (St Lucia Campus) operates, the Turrbal and Jagera people. We thank Angela Foerster for the helpful discussions.

## Appendix

### *A.1. Measurement probabilities*

Although the outcome probabilities for a measurement on an über-NOON state can be read from the state alone, to calculate any measurement probability for $|L,M,0,0;(\tau)\}$ we require the density matrix,

$$\rho(\tau)=|L,M,0,0;(\tau)\}\{L,M,0,0;(\tau)|.$$

Since we are only interested in the probabilities for the measurement outcomes on site 3, we can trace over the spaces labelled 2 and 4 to obtain a reduced density matrix,

$$\rho_{1,3}(\tau) = \sum_{l,l'=0}^{L}\sum_{m=0}^{M}\alpha_{l,m}(\tau)\,\alpha^{*}_{l',m}(\tau)\,|L-l,l\rangle\langle L-l',l'| + \frac{J^2}{16U^2(L-M+1)^2}\sum_{l,l'=0}^{L+1}\sum_{m=0}^{M-1}\beta_{l,m}(\tau)\,\beta^{*}_{l',m}(\tau)\,|L-l+1,l\rangle\langle L-l'+1,l'| + \frac{J^2}{16U^2(M-L+1)^2}\sum_{l,l'=0}^{L-1}\sum_{m=0}^{M+1}\gamma_{1,m}(\tau)\,\gamma^{*}_{l',m}(\tau)\,|L-l-1,l\rangle\langle L-l'-1,l'|.$$

Therefore at time $t=\tau$ given by (5), the probability of measuring $r$ number of bosons at site 3 is given by the expression

$$\begin{aligned}\mathbb{P}_3[r](\tau) = &\sum_{l,l'=0}^{L}\sum_{m=0}^{M}\alpha_{l,m}(\tau)\,\alpha^{*}_{l',m}(\tau)\,\{L-r,r|L-l,l\rangle\langle L-l',l'|L-r,r\} \\ &+\frac{J^2}{16U^2(L-M+1)^2}\sum_{l,l'=0}^{L+1}\sum_{m=0}^{M-1}\beta_{l,m}(\tau)\,\beta^{*}_{l',m}(\tau)\,\{L-r+1,r|L-l+1,l\rangle\langle L-l'+1,l'|L-r+1,r\} \\ &+\frac{J^2}{16U^2(M-L+1)^2}\sum_{l,l'=0}^{L-1}\sum_{m=0}^{M+1}\gamma_{1,m}(\tau)\,\gamma^{*}_{l',m}(\tau)\,\{L-r-1,r|L-l-1,l\rangle\langle L-l'-1,l'|L-r-1,r\},\end{aligned} \tag{34}$$

from which, by using the identities

$$\langle L-l,l|L,0\} = \sqrt{\frac{L!}{2^L(L-l)!l!}}, \quad \langle L-l,l|0,L\} = (-1)^l\sqrt{\frac{L!}{(L-l)!l!}},$$
$$\{1,L|L+1-l,l\rangle = (-1)^l(L+1-2l)\sqrt{\frac{L!}{2^{L+1}l!(L+1-l)!}},$$

we obtain the equations (25) and (26).

### *A.2. Damped oscillations in the large L, M limit*

Here we outline the argument as to why oscillations become negligible in the large $L,M$ limit. The calculations are split into a non-oscillating part, which is approximately the average of the curve as a function of $J^2/U^2$, and an oscillating part, which oscillates around this average. For example, when evaluating (25) we have the contribution:

$$\beta_{l,m}\beta^{*}_{l',m} = (L-l+1)\left(L-l'+1\right)\Bigg[\underbrace{\exp\left(i\pi\left(l'-l\right)\left(\frac{(N+1)}{2}-m\right)\right)}_{\text{non-oscillating}}$$
$$+\underbrace{\exp\left(i\pi\left(l'-l\right)\left(\frac{(N+1)}{2}-m\right)\frac{L-M-1}{L-M+3}\right)}_{\text{oscillating}}$$
$$-\underbrace{\exp\left(i\pi\left(l'-l\right)\left(\frac{(N+1)}{2}-m\right)\right)\exp\left(i\tau 4U(L-M+1)\right)z^{-(N+1)\left(l'+m\right)+2l'm+\sigma}}_{\text{oscillating}}$$
$$-\underbrace{\exp\left(i\pi\left(l'-l\right)\left(\frac{(N+1)}{2}-m\right)\right)\exp\left(-i\tau 4U(L-M+1)\right)z^{(N+1)(l+m)-2lm-\sigma}}_{\text{oscillating}}\Bigg]$$
$$\times\frac{L!M!}{2^{L+M}\sqrt{l!(L-l+1)!l'!(L-l'+1)!m!(M-m-1)!}}.$$

Applying the summations, we find that the non-oscillating part is a reducible term,

$$\sum_{l,l'=0}^{L+1}\sum_{m=0}^{M-1}\exp\left(\left(l'-l\right)\left(\frac{(N+1)}{2}-m\right)\right)\frac{(L+1)!L!M!}{2^{2L+M+1}l!\,(L-l)!l'!\,(L-l')!m!\,(M-m-1)!}$$
$$=\frac{M(L+1)}{8}.$$

However, the next term is more complicated,

$$\sum_{l,l'=0}^{L+1}\sum_{m=0}^{M-1}\exp\left(i\pi\left(l'-l\right)\left(\frac{(N+1)}{2}-m\right)\frac{L-M-1}{L-M+3}\right)\frac{(L+1)!L!M!}{2^{2L+M+1}l!\,(L-l)!l'!\,(L-l')!m!\,(M-m-1)!}$$
$$=\frac{M(L+1)}{2^{L+M+1}}\sum_{m=0}^{M-1}\left(1+\cos\left(\pi\left(\frac{(N+1)}{2}-m\right)\frac{L-M-1}{L-M+3}\right)\right)^{L}\frac{(M-1)!}{m!\,(M-m-1)!}.$$

Since $|\cos(x)|\leqslant 1$, we can consider the approximation

$$\left(1+\cos\left(\pi\left(\frac{(N+1)}{2}-m\right)\frac{L-M-1}{L-M+3}\right)\right)^{L}\approx 1+L\cos\left(\pi\left(\frac{(N+1)}{2}-m\right)\frac{L-M-1}{L-M+3}\right). \tag{35}$$

While this is not a good approximation for some values of $m$, $L$ and $M$, we still obtain a reasonable estimate by taking the sum over $m$ when $M$ is large. Using this approximation we have

$$\begin{aligned}
&\frac{M(L+1)}{2^{L+M+1}}\sum_{m=0}^{M-1}\left(1+(-1)^{\frac{(N+1)}{2}-m}\cos\left(\pi\left(\frac{(N+1)}{2}-m\right)\frac{4}{L-M+3}\right)\right)^{L}\frac{(M-1)!}{m!(M-m-1)!}\\
&\quad\approx\frac{M(L+1)}{2^{L+M+1}}\sum_{m=0}^{M-1}\left(1+L(-1)^{\frac{(N+1)}{2}-m}\cos\left(\pi\left(\frac{(N+1)}{2}-m\right)\frac{4}{L-M+3}\right)\right)\frac{(M-1)!}{m!(M-m-1)!}\\
&\quad<\frac{M(L+1)^2}{2^{L+M+1}}\sum_{m=0}^{M-1}\frac{(M-1)!}{m!(M-m-1)!}\\
&\quad=\frac{M(L+1)^2}{2^{L+2}}\xrightarrow[L\to\infty]{}0,
\end{aligned}\tag{36}$$

where we can determine that this term goes to zero in the limit $L$ approaching infinity; meaning we can ignore this term provided $L$ becomes sufficiently large. We can apply a similar analysis to the $\gamma_{l,m}\gamma^*_{l',m}$ terms. Again we have a reducible term, this simplifies to $L(M+2)/8$, and a second oscillating term,

$$\begin{aligned}
&\frac{L}{2^{L+M}}\sum_{m=0}^{M+1}\left(1+\cos\left(\pi\left(\frac{(N+1)}{2}-m\right)\frac{L-M+1}{L-M-3}\right)\right)^{L-1}\frac{(M-m+1)M!}{m!(M-m)!}\\
&\quad\approx\frac{L}{2^{L+M}}\sum_{m=0}^{M+1}\left(1+(L-1)\cos\left(\pi\left(\frac{(N+1)}{2}-m\right)\frac{L-M-1}{L-M-3}\right)\right)\frac{(M-m+1)M!}{m!(M-m)!}\\
&\quad<\frac{L^2}{2^{L+M}}\sum_{m=0}^{M+1}\frac{(M-m+1)M!}{m!(M-m)!}\\
&\quad=\frac{L^2(M+1)}{2^{L+1}}\xrightarrow[L\to\infty]{}0,
\end{aligned}\tag{37}$$

which also goes to zero. A similar argument can be made for all the other oscillating terms, where for large $L$ and $M$ these oscillations dampen around the average of the function. In practice, if (35) holds as an appropriate approximation and if the terms (36) and (37) become negligible then we can deem $L$ and $M$ to be *large* enough. These calculations illustrate how to identify the dominant terms arising from the triple summations. These dominant terms occur when the phase variables are integer multiples of $\pi/2$. When they are not, they can be neglected. We conclude that for the present calculation, there is only one dominant term, leading to

$$\begin{aligned}
&\sum_{l,l',m}\beta_{l,m}\beta^*_{l',m}\{L+1,0|L+1-l,l\rangle\langle L+1-l',l'|L+1,0\}\approx\frac{M(L+1)}{8},\\
&\sum_{l,l',m}\gamma_{l,m}\gamma^*_{l',m}\{L-1,0|L-1-l,l\rangle\langle L-1-l',l'|L-1,0\}\approx\frac{L(M+2)}{8},\\
&\sum_{l,l',m}\alpha_{l,m}\alpha^*_{l',m}\{L,0|L-l,l\rangle\langle L-l',l'|L,0\}\approx\frac{1}{2}-\frac{J^2}{16U^2(L-M+1)^2}\frac{M(L+2)}{4}\\
&\qquad\qquad-\frac{J^2}{16U^2(M-L+1)^2}\frac{L(M+2)}{4},
\end{aligned}$$

which ultimately provides a simplified expression for (25). In any case, these arguments can be applied to the other probability calculation (26) and the fidelity calculations (22), (27) and (28).

## ORCID iDs

Lachlan Bennett https://orcid.org/0000-0002-9283-383X
Phillip S Isaac https://orcid.org/0000-0001-8608-3940
Jon Links https://orcid.org/0000-0003-1049-0616

## References

[1] Lee H, Kok P and Dowling J P 2002 A quantum Rosetta stone for interferometry *J. Mod. Opt.* **49** 2325–38
[2] Slussarenko S, Weston M M, Chrzanowski H M, Shalm L K, Verma V B, Nam S W and Pryde G J 2017 Unconditional violation of the shot-noise limit in photonic quantum metrology *Nat. Photon.* **11** 700–3
[3] Pezzé L, Smerzi A, Oberthaler M K, Schmied R and Treutlein P 2018 Quantum metrology with nonclassical states of atomic ensembles *Rev. Mod. Phys.* **90** 035005
[4] Pelayo J C, Gietka K and Busch T 2023 Distributed quantum sensing with optical lattices *Phys. Rev.* A **107** 033318
[5] Pan J-W, Chen Z-B, Lu C-Y, Weinfurter H, Zeilinger A and Żukowski M 2012 Multiphoton entanglement and interferometry *Rev. Mod. Phys.* **84** 777
[6] Tóth G and Apellaniz I 2014 Quantum metrology from a quantum information science perspective *J. Phys. A: Math. Theor.* **47** 424006
[7] Afek I, Ambar O and Silberberg Y 2010 High-NOON states by mixing quantum and classical light *Science* **328** 879–81
[8] Israel Y, Rosen S and Silberberg Y 2014 Supersensitive polarization microscopy using NOON states of light *Phys. Rev. Lett.* **112** 103604
[9] Chen Y-A, Bao X-H, Yuan Z-S, Chen S, Zhao B and Pan J-W J 2010 Heralded generation of an atomic NOON state *Phys. Rev. Lett.* **104** 043601
[10] Lopes R, Imanaliev A, Aspect A, Cheneau M, Boiron D and Westbrook C I 2015 Atomic Hong-Ou-Mandel experiment *Nature* **520** 66–68
[11] Dowling J P 2008 Quantum optical metrology–the lowdown on high-NOON states *Contemp. Phys.* **49** 125–43
[12] Sanders B C 1989 Quantum dynamics of the nonlinear rotator and the effects of continual spin measurement *Phys. Rev.* A **40** 2417
[13] Boto A N, Kok P, Abrams D S, Braunstein S L, Williams C P and Dowling J P 2000 Quantum interferometric optical lithography: exploiting entanglement to beat the diffraction limit *Phys. Rev. Lett.* **85** 2733
[14] Walther P, Pan J-W, Aspelmeyer M, Ursin R, Gasparoni S and Zeilinger A 2004 De Broglie wavelength of a non-local four-photon state *Nature* **429** 158–61
[15] Mitchell M W, Lundeen J S and Steinberg A M 2004 Super-resolving phase measurements with a multiphoton entangled state *Nature* **429** 161–4
[16] Zhang J, Um M, Lv D, Zhang J-N, Duan L-M and Kim K 2018 NOON states of nine quantized vibrations in two radial modes of a trapped ion *Phys. Rev. Lett.* **121** 160502
[17] Soto-Eguibar F and Moya-Cessa H M 2019 Generation of NOON states in waveguide arrays *Ann. Phys.* **531** 1900250
[18] Bychek A A, Maksimov D N and Kolovsky A R 2018 NOON state of bose atoms in the double-well potential via an excited-state quantum phase transition *Phys. Rev.* A **97** 063624
[19] Vanhaele G and Schlagheck P 2021 NOON states with ultracold bosonic atoms via resonance- and chaos-assisted tunneling *Phys. Rev.* A **103** 013315
[20] Vanhaele G, Bäcker A, Ketzmerick R and Schlagheck P 2022 Creating triple-NOON states with ultracold atoms via chaos-assisted tunneling *Phys. Rev.* A **106** L011301
[21] Cao D-Z, Zhang X-Z, Wang C, Ren C, Zhang J, Li Z, Zhang S-H and Wang K 2023 NOON-state generation and superresolved interference in a double-slit experiment *Phys. Rev.* A **107** 022417
[22] Qi S-F and Jing J 2023 Floquet generation of a magnonic NOON state *Phys. Rev.* A **107** 013702
[23] Li C, Sampuli E M, Song J, Xia Y and Ding W 2018 One-step engineering many atom NOON state *New J. Phys.* **20** 093019
[24] Qi S-F and Jing J 2023 Generating entangled states from coherent states in circuit-QED *Phys. Rev.* A **107** 042412

[25] Grün D S, Wittmann K, Ymai W L H, Links J and Foerster A 2022 Protocol designs for NOON states *Commun. Phys.* **5** 36
[26] Grün D S, Ymai L H, Wittmann K Tonel W A P, Foerster A and Links J 2022 Integrable atomtronic interferometry *Phys. Rev. Lett.* **129** 020401
[27] Kitagawa M and Ueda M 1993 Squeezed spins states *Phys. Rev.* A **47** 5138
[28] Alexander B, Bollinger J J and Uys H 2020 Generating Greenberger-Horne-Zeilinger states with squeezing and postselection *Phys. Rev.* A **101** 062303
[29] Plodzień M, Lewenstein M, Witkowska E and Chwedeńczuk J 2022 One-axis twisting as a method of generating many-body bell correlations *Phys. Rev. Lett.* **129** 250402
[30] Tonel A P, Ymai L H, Foerster A and Links J 2015 Integrable model of bosons in a four-well ring with anisotropic tunneling *J. Phys. A: Math. Theor.* **48** 494001
[31] Lahaye T, Menotti C, Santos L, Lewenstein M and Pfau T 2009 The physics of dipolar bosonic quantum gases *Rep. Prog. Phys.* **72** 126401
[32] Bloch I 2005 Ultracold quantum gases in optical lattices *Nat. Phys.* **1** 23–30
[33] Baranov M A 2008 Theoretical progress in many-body physics with ultracold dipolar gases *Phys. Rep.* **464** 71–111
[34] Ymai L H, Tonel A P, Foerster A and Links J 2017 Quantum integrable multi-well tunneling models *J. Phys. A: Math. Theor.* **50** 264001
[35] Seaman B T, Krämer M, Anderson D Z and Holland M J 2007 Atomtronics: ultracold-atom analogs of electronic devices *Phys. Rev.* A **75** 023615
[36] Migliore A and Messina A 2022 Quantum optics parity effect on generalized NOON states and its implications for quantum metrology *Ann. Phys.* **534** 2200304
[37] Giovannetti V, Lloyd S and Maccone L 2004 Quantum-enhanced measurements: beating the standard quantum limit *Science* **306** 1330–6
[38] Links J and Hibberd K E 2006 Bethe ansatz solutions of the Bose-Hubbard dimer *SIGMA* **2** 095